Human Molecular Genetics, 2009, Vol. 18, No. 23 ***4546–4551***
doi:10.1093/hmg/ddp416
Advance Access published on September 4, 2009

Pathogenic NAP57 mutations decrease ribonucleoprotein assembly in dyskeratosis congenita

Petar N. Grozdanov[1,†], Narcis Fernandez-Fuentes[2,3,‡], Andras Fiser[2,3] and U. Thomas Meier[1,*]

[1]Department of Anatomy and Structural Biology, [2]Department of Systems and Computational Biology and [3]Department of Biochemistry, Albert Einstein College of Medicine, 1300 Morris Park Avenue, Bronx, NY 10461, USA

Received July 20, 2009; Revised August 13, 2009; Accepted August 26, 2009

X-linked dyskeratosis congenita (DC) is a rare bone marrow failure syndrome caused by mostly missense mutations in the pseudouridine synthase NAP57 (dyskerin/Cbf5). As part of H/ACA ribonucleoproteins (RNPs), NAP57 is important for the biogenesis of ribosomes, spliceosomal small nuclear RNPs, microRNAs and the telomerase RNP. DC mutations concentrate in the N- and C-termini of NAP57 but not in its central catalytic domain raising questions as to their impact. We demonstrate that the N- and C-termini together form the binding surface for the H/ACA RNP assembly factor SHQ1 and that DC mutations modulate the interaction between the two proteins. Pinpointing impaired interaction between NAP57 and SHQ1 as a potential molecular basis for X-linked DC has implications for therapeutic approaches, e.g. by targeting the NAP57–SHQ1 interface with small molecules.

INTRODUCTION

Dyskeratosis congenita (DC) is a rare inherited bone marrow failure syndrome characterized by the cutaneous triad of nail dystrophy, abnormal skin pigmentation and mucosal leukoplakia, causing premature death due to aplastic anemia (1). Although in many cases the genes affected remain to be identified, the predominant X-linked form is caused by mutations in the pseudouridine synthase, NAP57 (aka dyskerin or Cbf5p in yeast and Cbf5 in archaea), of H/ACA ribonucleoproteins (RNPs) (2,3). The autosomal dominant and recessive forms trace to mutations in two additional H/ACA RNP core proteins, NOP10 and NHP2, in telomerase reverse transcriptase and RNA, and in the telomeric shelterin component TIN2. Given that telomerase belongs to the family of H/ACA RNPs and all DC patients exhibit shortened telomeres in their peripheral blood cells, DC is considered a telomere deficiency (1). Nevertheless, it is contentious to what degree impairment of the functions of the other 150 or so H/ACA RNPs, e.g. ribosomal RNA and spliceosomal small nuclear RNA modification, contribute to the pathological features of DC (4,5). Importantly, the molecular impact of none of the identified mutations in any of the affected genes has been elucidated. Here we demonstrate that the mutations in NAP57 modulate its interaction with SHQ1, one of the assembly factors of H/ACA RNPs.

H/ACA RNPs consist of two sets of four core proteins, each set assembling around one of two hairpins of a function determining H/ACA RNA (6). In most cases, H/ACA RNAs guide site-directed pseudouridylation of target RNAs by base pairing (7). Other H/ACA RNAs, such as telomerase RNA, which ends in an H/ACA domain, lack complementarity to any stable RNAs (8). NAP57 together with NOP10 and NHP2 forms a core trimer that is essential for the stability of all H/ACA RNPs. A fourth H/ACA core protein, GAR1, interacts with NAP57 independently (9). A hairpin of an H/ACA RNA stretches across the relatively planar surface of the core trimer anchored with its 3′-end in the PUA domain of NAP57 and with its terminal loop in NHP2 (10). The mostly missense mutations in NAP57 identified in X-linked DC patients concentrate in its N-terminal (NT) and C-terminal (CT) domains mostly avoiding the central catalytic domain (Fig. 2A) (11). In models of the three-dimensional structure of human NAP57, the mutated domains wrap around each

*To whom correspondence should be addressed. Tel: +1 7184303294; Fax: +1 7184308996; Email: meier@aecom.yu.edu
†Present address: Cell Biology and Biochemistry, Texas Tech University Health Sciences Center, 3601 4th Street, Lubbock, TX 79430, USA.
‡Present address: Leeds Institute of Molecular Medicine, Section of Experimental Therapeutics, University of Leeds, St James's University Hospital, Wellcome Trust Brenner Building, Leeds LS9 7TF, UK.

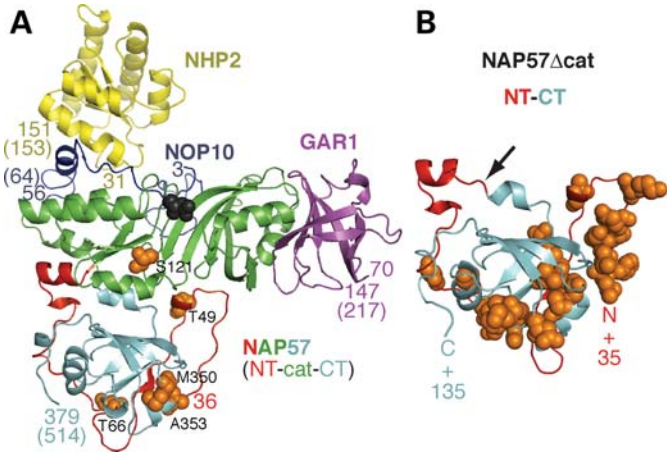

Figure 1. Models of human H/ACA core complex protein structures. (**A**) Entire human H/ACA protein core complex modeled as described in the text. The protein only complex consists of NHP2 (yellow), NOP10 (dark blue), GAR1 (magenta) and NAP57 (red–green–cyan for the N-terminal, catalytic and C-terminal domain, respectively). Space filling models identify the amino acids mutated in this study according to mutations observed in X-linked DC (orange) and the catalytic aspartate (black). To indicate how much of the actual protein sequences are missing, the starting and ending positions are indicated (including the number of residues of the full-length proteins). (**B**) Spliced N- (red) and C-termini (cyan) of NAP57 representing the NAP57Δcat construct generated for this study. It concentrates 32 of 35 mutation sites identified in NAP57 of X-linked DC-patients (Fig. 2A); 21 are present in the structure (orange). The splice junction between N- and C-termini is indicated (arrow).

other forming a contiguous mutation cluster (Fig. 1) (10,12). Surprisingly, this DC mutation cluster is not part of any intra-RNP molecular interactions consequently it must be contacting a yet to be identified factor. Here, we identify the H/ACA RNP assembly factor SHQ1 as the protein specifically binding to the NAP57 domains forming the DC mutation cluster.

RESULTS

We previously demonstrated that SHQ1 binds NAP57 making it a candidate for a factor interacting with the DC mutation cluster of NAP57 (13). However, testing this hypothesis required the fusion of the NT and CT domains of NAP57 forming the mutation cluster while excising its catalytic domain. To achieve this goal without disrupting the tertiary structure of the mutation cluster, we modeled the structure of human NAP57 based on those of the crystal structures of archaeal H/ACA RNPs. Archaeal H/ACA RNPs differ from mammalian ones in that their NHP2 ortholog, L7Ae, independently recognizes archaeal H/ACA RNAs, whereas NHP2 together with the other H/ACA core proteins can form a protein only complex (9,10). Therefore, we modeled this human complex by docking NHP2, modeled according to the structure of the related 15.5 K protein (14), onto the NOP10–NAP57–GAR1 complex, as described in Materials and Methods (Fig. 1A). In the model of human NAP57 derived from this complex, we identified two helices at the NT and CT of the catalytic domain that were in close proximity to each other. Specifically, fusion of the residues G90 and P288, which are only 5.05 Å apart, would generate a new protein, NAP57Δcat, with minimal impact on the tertiary structure of its CT PUA domain benefitting from the fact that Gly-Pro motifs are commonly found in naturally occurring kinked helices (Fig. 1B) (15). Thus, we designed and computationally assessed the feasibility (see Materials and Methods) of a NAP57 construct, NAP57Δcat, that lacked its catalytic domain but retained most DC mutation sites (Figs 1B and 2A).

To experimentally address if the NAP57Δcat construct folded properly, it was expressed in bacteria as a fusion with the maltose binding protein (MBP, Fig. 2A) and tested in amylose resin pull-down assays (13). Specifically, we investigated if MBP-NAP57Δcat (and additional constructs, Fig. 2A) retained the ability of full-length NAP57 to interact with recombinant SHQ1 (Fig. 2B). All constructs containing the CT domain of NAP57 bound SHQ1 (Fig. 2B, lanes 8–10), whereas the catalytic domain (cat, lane 7) or the NT alone did not (Fig. 2C, lane 4). To further explore the contribution of the Δcat NT to the interaction with SHQ1, binding of SHQ1 to Δcat and to the CT alone was compared at increasing salt concentrations (Fig. 2D). Binding was clearly enhanced by the presence of the NT, which was particularly evident at 210 mM salt (Fig. 2D, compare lanes 5 and 6, inset). This result was corroborated when investigated in the context of the cell nucleus using an *in vivo* nuclear tethering assay (16). Specifically, when tethered (by a Lac repressor fusion domain, LacI) to Lac operator arrays integrated in the genome, Δcat recruited endogenous SHQ1 efficiently (Fig. 2E, 84% of cells, $n = 50$), whereas the CT alone failed to do so (Fig. 2F, 79% of cells, $n = 68$). These data indicated that the NT folded properly around the CT in our NAP57Δcat construct and that both domains concentrating most DC mutation sites were required for full interaction with SHQ1. In conclusion, SHQ1 bound to the DC mutation cluster.

SHQ1 consists of an HSP20-like NT CS domain and a unique CT (Fig. 3A) (13,17,18). We tested if SHQ1 lacking its CS domain, SHQ1ΔCS, bound to NAP57Δcat, because it was this domain that interacted with full-length NAP57 (13). Indeed, SHQ1ΔCS interacted with NAP57Δcat (Fig. 3B), whereas the CS domain alone failed to do so (Fig. 3C) further supporting proper folding of the NAP57Δcat construct. Moreover, recruitment of endogenous SHQ1 to sites of NAP57Δcat concentration in the nucleus (Fig. 2E) was specific, because Δcat failed to recruit another H/ACA RNP assembly factor, NAF1 (Fig. 3D), and because the catalytic domain alone did not recruit SHQ1 (Fig. 3E). Finally, when cotransfected with NAP57Δcat, the normally cytoplasmic SHQ1-LacI (13) was ferried quantitatively into the nucleus [presumably by the abundance of nuclear localization signals in the NAP57Δcat domains (19)] where it concentrated together with Δcat in nucleoli and at Lac operator sites (Fig. 3F). Together, these data provide further evidence for a specific interaction between SHQ1ΔCS and NAP57Δcat.

Our data showed that SHQ1 bound to the NAP57 domains harboring most of the mutation sites identified in X-linked DC patients (Figs 1–3). Therefore, we tested whether DC mutations interfered with SHQ1 binding. The predominant mutation in X-linked DC is a mutation of alanine 353 to valine (A353V), accounting for ~40% of all cases (11). Owing to the close relatedness of alanine and valine, we

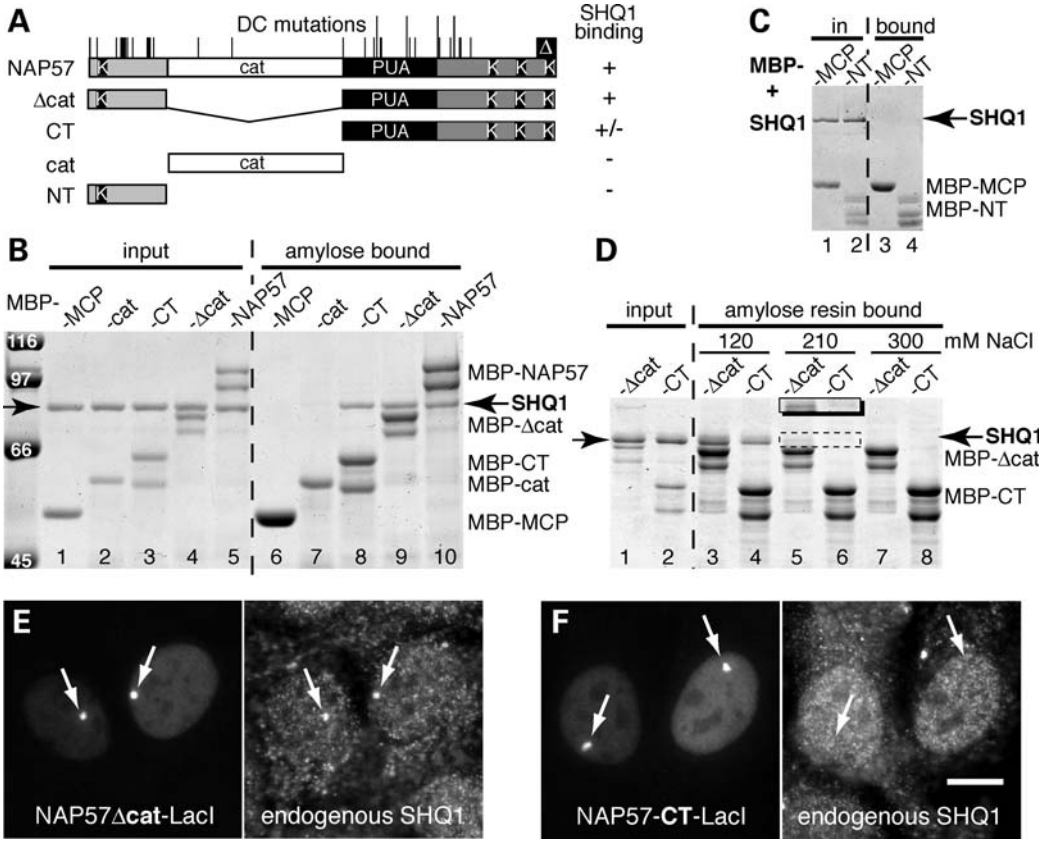

Figure 2. SHQ1 binds to the spliced N- (NT) and C-termini (CT) of NAP57 (NAP57Δcat) that concentrates most DC mutation sites. (**A**) Schematic of constructs. The location of DC mutations is indicated above NAP57 (bars) including those that are mutated to two different amino acids (double height) and a C-terminal deletion (Δ). Note the Δcat construct with the catalytic domain (cat) excised but retaining the RNA binding pseudouridylase and archaeosine transglycosylase (PUA) domain. Positively charged stretches that double as nuclear localization signals are indicated (K). (**B** and **C**) Recombinant proteins fused to the maltose binding protein (MBP) were mixed with SHQ1 (arrows), retained on amylose resin and analyzed on Coomassie blue stained SDS–polyacrylamide gels before (input, 10%) and after retention (bound). As previously observed for full-length NAP57 (13), every construct containing its CT migrated as two bands (in the case of MBP-NT, the lower bands were breakdown products). The bacteriophage MS2 coat protein (MCP) was included as a control. (**D,** inset) Enhanced contrast of region identified by dashed box below demonstrating increased binding of SHQ1 with the NT present. (**E** and **F**) Nuclear tethering assay: double immunofluorescence of constructs fused to LacI, which are transfected and tethered to lac operator repeats stably integrated into the genome (arrows) and which do (E) or do not (F) recruit endogenous SHQ1. Bar = 10 μm.

first investigated the binding of a more divergent but artificial A353R mutation under increasing salt concentrations. Surprisingly, NAP57 A353R retained SHQ1 markedly better on amylose resin than wild-type NAP57 (Fig. 4A), which was particularly conspicuous in the presence of 210 mM salt (compare lanes 5 and 6). Subsequent testing of the A353V patient mutation also showed it bound more SHQ1 than the wild-type, although not quite as noticeably (Fig. 4B). However, quantification of the gel bands revealed a near two-fold (1.7 ± 0.4, $n = 3$) increase of the SHQ1/NAP57 ratio between wild-type and A353V mutant NAP57 (Fig. 4B). Therefore, this patient mutation enhances the affinity of NAP57 for its assembly factor SHQ1. Interestingly, testing of additional patient mutants revealed some with decreased affinity for SHQ1 (Fig. 4C). Specifically, when compared with binding of wild-type NAP57 (Fig. 4C, lane 1) that of the T66A and M350T mutants was reduced (lane 3 and 6), whereas that of the T49M and M350I mutants was enhanced (lanes 2 and 5). Notably, the mutation of methionine 350 of NAP57 to isoleucine (M350I) increased affinity for SHQ1, whereas that to threonine (M350T) decreased it (Fig. 4C, compare lanes 5 and 6). In contrast, mutation of serine 121 to glycine barely impacted SHQ1 binding, consistent with the location of that serine in the center of the catalytic domain, which is not required for SHQ1 binding. Therefore, the S121G mutation may primarily affect the catalytic activity of NAP57 rather than the biogenesis of H/ACA RNPs. Regardless, our data demonstrate that DC mutations generally impact the interaction between NAP57 and the H/ACA RNP assembly factor SHQ1 in a hypo- or hypermorphic fashion marking X-linked DC as a potential RNP assembly deficiency.

DISCUSSION

X-linked DC is caused by mutations in NAP57, a core protein of all H/ACA RNPs. These mostly missense mutations concentrate in the same three-dimensional domain formed by the NT and CT of the protein. In a model of human H/ACA RNPs, the mutated amino acids do not compromise RNP

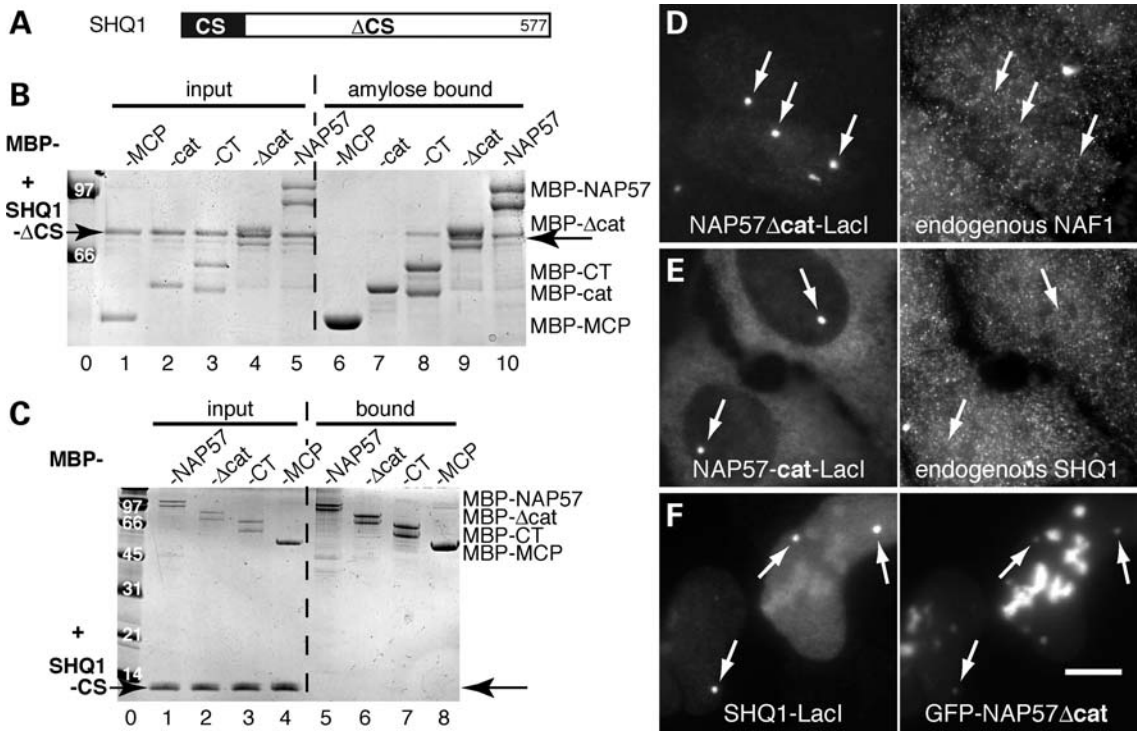

Figure 3. The CS domain of SHQ1 is not required for NAP57Δcat binding. (**A**) Schematic of SHQ1 highlighting its HSP20-like CS domain. (**B** and **C**) MBP-fusion protein retention assays as in Figure 2B–D but using SHQ1ΔCS (B, arrows) and the SHQ1-CS domain alone (C, arrows). Conditions and abbreviations are in Figure 2D–F. Nuclear tethering assays (Fig. 2E and F) with the indicated constructs. Bar = 10 μm.

integrity directly, as they are not contacting any other proteins of the particle nor the H/ACA RNA. In contrast, we document that the DC mutations impact the interaction of NAP57 with the H/ACA RNP assembly factor SHQ1.

To understand how both increased and decreased affinity of NAP57 for SHQ1 has the same dire consequences, it is important to consider the relationship and function of the two proteins.

SHQ1 functions in an obligate early step of H/ACA RNP biogenesis (13). Specifically, SHQ1 binds to newly synthesized NAP57, stabilizing it and preventing it from misfolding and degradation. In support of this notion, excess SHQ1 inhibits RNP assembly by sequestration of NAP57 and depletion of SHQ1 causes a loss of NAP57 due to degradation (13,20). Therefore, both increase and decrease of SHQ1 share the same consequence, reduced availability of NAP57 for RNP assembly. Apparently, SHQ1 and NAP57 live in a yin–yang relationship with specific cellular levels of each being crucial to cell viability. We now demonstrate that X-linked DC mutations cause an imbalance in the delicate relationship of NAP57 and SHQ1 by modulating their affinity for each other and thereby impairing H/ACA RNP biogenesis. Whether the effect is more dramatic on some H/ACA RNPs (e.g. telomerase) than others, remains to be determined but appears likely given the specific reduction of telomerase RNA and telomere length in DC patient cells (2).

There is ample evidence for diminished levels of NAP57 causing DC and other phenotypes. For example, DC mutations in the NAP57 gene have been identified in its promoter and in introns; apparently, all causing reduced expression (21,22). Moreover, a mouse model of X-linked DC is hypomorphic for NAP57 (23) and reduced expression of the yeast NAP57 ortholog, Cbf5p, suppresses tRNA-mediated gene silencing (24). Here we find that DC mutations in NAP57, whether hyper- or hypomorphic, reduce its availability for RNP assembly. In summary, our data show that through physical interaction SHQ1 is an important regulator of cellular levels of free NAP57 and that modulation of this interaction forms a potential molecular basis for X-linked DC. Having pinpointed this interaction surface as the culprit in X-linked DC makes it amenable to small molecule screens for future therapeutic approaches.

MATERIALS AND METHODS

Modeling of human H/ACA core proteins

The human GAR1–NAP57–NOP10 complex was modeled using the archaeal 2apo (25) and 2ey4 (12) structures and NHP2 using the structure of the related 15.5K protein 1e7k (14) as templates following our previously described protocol (26). The structural model of the entire H/ACA core protein complex was obtained using the following three steps. First, NHP2 was blindly docked onto the GAR1–NAP57–NOP10 complex (i.e. non-biased docking) using FT-dock 2.0 (27). The search yielded a sampling space composed of more than 10 000 docking poses that exhibited the best surface complementarity between GAR1–NAP57–NOP10 and NHP2. Secondly, more than 250 docking poses located in a region close to NOP10 (i.e. NHP2 docking poses whose center of

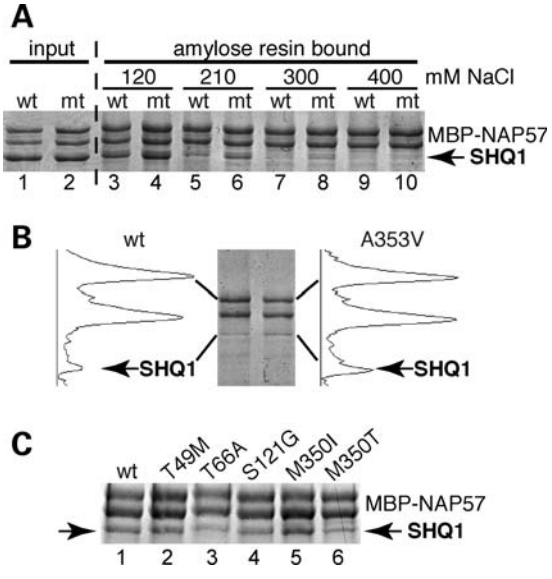

Figure 4. Amino acid changes observed in NAP57 of DC patients modulate its interaction with SHQ1. MBP retention assays with mutant NAP57 (see legend to Fig. 2B–D). (**A**) Wild-type (wt) and an A353R mutant NAP57 (mt) fused to MBP were used to retain SHQ1 under increasing salt concentrations. Note the increased binding of the mutant. (**B**) The fractions retained with wild-type (left) or mutant MBP-NAP57 (A353V, right) were analyzed by SDS–PAGE and the Coomassie blue stained lanes scanned and enlarged (left and right of the gel). Note the increased binding of the mutant accounting for ~40% of all X-linked DC cases. (**C**) The fractions retained with the NAP57 variants indicated above as in (B). Note the increased (lanes 2 and 5) and reduced binding (lanes 3 and 6) of certain mutants relative to wild-type NAP57 (lane 1).

mass was contained within a distance of 10 Å to any residue of NOP10) were selected, because we previously showed NOP10 to be required for NHP2 binding (9). Thirdly, because 1e7k (14), the template used to model NHP2, was co-crystallized with RNA, we requested that the equivalent structural region in NHP2 be exposed and oriented consistently to the RNA binding region of the NOP10–NAP57–GAR1 complex, reducing the number of docking poses to 45. The remaining docking poses were rescored by using statistical potentials (28) and further refined using MultiDock (29). The top 20 docking poses were visually inspected and the top-scoring pose, which oriented the RNA binding regions of NHP2 and GAR1–NAP57–NOP10 in the same plane, was selected (Fig. 1A).

The viability of NAP57Δcat was confirmed by computational means as follows. Two structural models of NAP57Δcat were built using NAP57 as template by linking G90 to P288 either directly (G90-P288) or by an intermediate glycine (G90-G-P288). To assess the structural integrity of the models, a short molecular dynamic simulation was performed. The models were minimized and simulated during 2 ns in implicit solvent (GBSA) (30) using AMBER ff99 force-field (31) in the TINKER molecular modeling package (http ://dasher.wustl.edu/tinker). The structural models remained stable throughout the simulation, i.e. all intermediate conformational snapshots dumped during the simulation had a root mean square deviation of less than 2.5 Å (Cα) upon structural superposition of the initial models (i.e. prior to simulation). The quality of the models was evaluated using ProSa (32). Both models, G90-P288 and G90-G-P288, had comparable ProSa Zscores, −4.24 and −4.45, respectively. Lower ProSa Zscores indicate more stable structures and both scores fell within the typical range of native proteins of similar size. The models in Figure 1 were generated using MacPyMOL (www.pymol.org).

DNA constructs and expression, and protein–protein interaction assays

Most constructs and methods have been described previously (13). For bacterial expression, the following MBP-fusions were constructed: MBP-NT (pPG65, first 90 amino acids of NAP57), MBP-cat (pPG48, amino acids 91–287 corresponding to catalytic domain of NAP57), MBP-CT (pPG33, amino acids 289–514 constituting the CT of NAP57) and MBP-NAP57Δcat (pPG32, NAP57 with its catalytic domain excised, pSR55, fusion of amino acids 90–287). Unlike the full-length MBP-NAP57, pPG17 (13), these constructs lacked a CT hexa-histidine tag. All NAP57 point mutants were identical to full-length MBP-NAP57 (with a CT hexa-histidine tag) and generated by site-directed mutagenesis directly in pPG17, T49M (pPG59), T66A (pPG63), M350I (pPG61), M350T (pPG60) or in a different vector first, S121G (pPG62, pSR44), A353R (pPG53, pSR47) and A353V (pPG51, pSR45). Codon replacement of all NAP57 mutants was verified by sequencing. For transient expression in tissue culture cells, some of the NAP57 constructs above were fused to the lac-repressor (LacI) and to monomeric GFP: LacI-cat (pPG49), LacI-CT (pPG30), LacI-NAP57Δcat (pPG23) and GFP-NAP57Δcat (pSRS29).

Transient transfection, bacterial protein expression and purification, and protein–protein interactions *in vitro* (amylose resin pull-downs) and *in vivo* (nuclear tethering assay) were as we described previously (13,16). Gel bands were quantified using NIH ImageJ software.

ACKNOWLEDGEMENTS

We are grateful to Sujayita Roy and Sudhamani Ramamurthy for construction of some of the plasmids and to Susan Smith for critical comments on the manuscript.

Conflict of Interest statement. None declared.

FUNDING

This work was supported by a grant from the National Institutes of Health (HL079566) to U.T.M.

REFERENCES

1. Walne, A.J. and Dokal, I. (2009) Advances in the understanding of dyskeratosis congenita. *Br. J. Haematol.*, **145**, 164–172.
2. Mitchell, J.R., Wood, E. and Collins, K. (1999) A telomerase component is defective in the human disease dyskeratosis congenita. *Nature*, **402**, 551–555.
3. Heiss, N.S., Knight, S.W., Vulliamy, T.J., Klauck, S.M., Wiemann, S., Mason, P.J., Poustka, A. and Dokal, I. (1998) X-linked dyskeratosis

congenita is caused by mutations in a highly conserved gene with putative nucleolar functions. *Nat. Genet.*, **19**, 32–38.
4. He, J., Gu, B.W., Ge, J., Mochizuki, Y., Bessler, M. and Mason, P.J. (2009) Variable expression of Dkc1 mutations in mice. *Genesis*, **47**, 366–373.
5. Yoon, A., Peng, G., Brandenburger, Y., Zollo, O., Xu, W., Rego, E. and Ruggero, D. (2006) Impaired control of IRES-mediated translation in X-linked dyskeratosis congenita. *Science*, **312**, 902–906.
6. Meier, U.T. (2005) The many facets of H/ACA ribonucleoproteins. *Chromosoma*, **114**, 1–14.
7. Kiss, T. (2002) Small nucleolar RNAs: an abundant group of noncoding RNAs with diverse cellular functions. *Cell*, **109**, 145–148.
8. Mitchell, J.R., Cheng, J. and Collins, K. (1999) A box H/ACA small nucleolar RNA-like domain at the human telomerase RNA 3′ end. *Mol. Cell. Biol.*, **19**, 567–576.
9. Wang, C. and Meier, U.T. (2004) Architecture and assembly of mammalian H/ACA small nucleolar and telomerase ribonucleoproteins. *EMBO J.*, **23**, 1857–1867.
10. Li, L. and Ye, K. (2006) Crystal structure of an H/ACA box ribonucleoprotein particle. *Nature*, **443**, 302–307.
11. Vulliamy, T.J. and Dokal, I. (2008) Dyskeratosis congenita: the diverse clinical presentation of mutations in the telomerase complex. *Biochimie*, **90**, 122–130.
12. Rashid, R., Liang, B., Baker, D.L., Youssef, O.A., He, Y., Phipps, K., Terns, R.M., Terns, M.P. and Li, H. (2006) Crystal structure of a Cbf5–Nop10–Gar1 complex and implications in RNA-guided pseudouridylation and dyskeratosis congenita. *Mol. Cell*, **21**, 249–260.
13. Grozdanov, P.N., Roy, S., Kittur, N. and Meier, U.T. (2009) SHQ1 is required prior to NAF1 for assembly of H/ACA small nucleolar and telomerase RNPs. *RNA*, **15**, 1188–1197.
14. Vidovic, I., Nottrott, S., Hartmuth, K., Luhrmann, R. and Ficner, R. (2000) Crystal structure of the spliceosomal 15.5kD protein bound to a U4 snRNA fragment. *Mol. Cell*, **6**, 1331–1342.
15. Fernandez-Fuentes, N., Querol, E., Aviles, F.X., Sternberg, M.J. and Oliva, B. (2005) Prediction of the conformation and geometry of loops in globular proteins: testing ArchDB, a structural classification of loops. *Proteins*, **60**, 746–757.
16. Darzacq, X., Kittur, N., Roy, S., Shav-Tal, Y., Singer, R.H. and Meier, U.T. (2006) Stepwise RNP assembly at the site of H/ACA RNA transcription in human cells. *J. Cell Biol.*, **173**, 207–218.
17. Singh, M., Gonzales, F.A., Cascio, D., Heckmann, N., Chanfreau, G. and Feigon, J. (2009) Structure and functional studies of the CS domain of the essential H/ACA ribonucleoparticle assembly protein SHQ1. *J. Biol. Chem.*, **284**, 1906–1916.
18. Shirasu, K., Lahaye, T., Tan, M.W., Zhou, F., Azevedo, C. and Schulze-Lefert, P. (1999) A novel class of eukaryotic zinc-binding proteins is required for disease resistance signaling in barley and development in C. elegans. *Cell*, **99**, 355–366.
19. Meier, U.T. and Blobel, G. (1994) NAP57, a mammalian nucleolar protein with a putative homolog in yeast and bacteria. *J. Cell Biol.*, **127**, 1505–1514, [Correction appeared in 140: 447].
20. Yang, P.K., Rotondo, G., Porras, T., Legrain, P. and Chanfreau, G. (2002) The Shq1p.Naf1p complex is required for box H/ACA small nucleolar ribonucleoprotein particle biogenesis. *J. Biol. Chem.*, **277**, 45235–45242.
21. Salowsky, R., Heiss, N.S., Benner, A., Wittig, R. and Poustka, A. (2002) Basal transcription activity of the dyskeratosis congenita gene is mediated by Sp1 and Sp3 and a patient mutation in a Sp1 binding site is associated with decreased promoter activity. *Gene*, **293**, 9–19.
22. Knight, S.W., Vulliamy, T.J., Morgan, B., Devriendt, K., Mason, P.J. and Dokal, I. (2001) Identification of novel DKC1 mutations in patients with dyskeratosis congenita: implications for pathophysiology and diagnosis. *Hum. Genet.*, **108**, 299–303.
23. Ruggero, D., Grisendi, S., Piazza, F., Rego, E., Mari, F., Rao, P.H., Cordon-Cardo, C. and Pandolfi, P.P. (2003) Dyskeratosis congenita and cancer in mice deficient in ribosomal RNA modification. *Science*, **299**, 259–262.
24. Kendall, A., Hull, M.W., Bertrand, E., Good, P.D., Singer, R.H. and Engelke, D.R. (2000) A CBF5 mutation that disrupts nucleolar localization of early tRNA biosynthesis in yeast also suppresses tRNA gene-mediated transcriptional silencing. *Proc. Natl Acad. Sci. USA*, **97**, 13108–13113.
25. Hamma, T., Reichow, S.L., Varani, G. and Ferre-D'Amare, A.R. (2005) The Cbf5-Nop10 complex is a molecular bracket that organizes box H/ACA RNPs. *Nat. Struct. Mol. Biol.*, **12**, 1101–1107.
26. Fernandez-Fuentes, N., Rai, B.K., Madrid-Aliste, C.J., Fajardo, J.E. and Fiser, A. (2007) Comparative protein structure modeling by combining multiple templates and optimizing sequence-to-structure alignments. *Bioinformatics*, **23**, 2558–2565.
27. Gabb, H.A., Jackson, R.M. and Sternberg, M.J. (1997) Modelling protein docking using shape complementarity, electrostatics and biochemical information. *J. Mol. Biol.*, **272**, 106–120.
28. Moont, G., Gabb, H.A. and Sternberg, M.J. (1999) Use of pair potentials across protein interfaces in screening predicted docked complexes. *Proteins*, **35**, 364–373.
29. Jackson, R.M., Gabb, H.A. and Sternberg, M.J. (1998) Rapid refinement of protein interfaces incorporating solvation: application to the docking problem. *J. Mol. Biol.*, **276**, 265–285.
30. Still, W. and Tempczyck, A. (1990) A semiempirical treatment of solvation for molecualr mechanics and dynamics. *J. Am. Chem. Soc.*, **112**, 6127–6129.
31. Wang, J.M., Cieplak, P. and Kollman, P.A. (2000) AMBER ff99. *J. Comput. Chem.*, **21**, 1049–1074.
32. Sippl, M.J. (1993) Recognition of errors in three-dimensional structures of proteins. *Proteins*, **17**, 355–362.